Available online at www.sciencedirect.com
ScienceDirect
Journal of Power Sources 159 (2006) 1328–1333
JOURNAL OF POWER SOURCES
www.elsevier.com/locate/jpowsour

Synthesis and electrochemical properties of $Li[Ni_{0.8}Co_{0.1}Mn_{0.1}]O_2$ and $Li[Ni_{0.8}Co_{0.2}]O_2$ via co-precipitation

Myung-Hyoon Kim [a], Ho-Suk Shin [a], Dongwook Shin [b], Yang-Kook Sun [a,*]

[a] *Department of Chemical Engineering, Center for Information and Communication Materials, Hanyang University, Seoul 133-791, South Korea*
[b] *Division of Material Science and Engineering, Center for Information and Communication Materials, Hanyang University, Seoul 133-791, South Korea*

Received 23 October 2005; received in revised form 26 November 2005; accepted 29 November 2005
Available online 18 January 2006

Abstract

Spherical $Li[Ni_{0.8}Co_{0.2-x}Mn_x]O_2$ ($x = 0$, 0.1) with phase-pure and well-ordered layered structure have been synthesized by heat-treatment of spherical $[Ni_{0.8}Co_{0.2-x}Mn_x](OH)_2$ and $LiOH{\cdot}H_2O$ precursors. The structure, morphology, electrochemical properties, and thermal stability of $Li[Ni_{0.8}Co_{0.2-x}Mn_x]O_2$ ($x = 0$, 0.1) were studied. The average particle size of the powders was about 10–15 μm and the size distribution was narrow due to the homogeneity of the metal hydroxide $[Ni_{0.8}Co_{0.2-x}Mn_x](OH)_2$ ($x = 0$, 0.1). The $Li[Ni_{0.8}Co_{0.2-x}Mn_x]O_2$ ($x = 0$, 0.1) delivered a discharge capacity of 197–202 mAh g^{-1} and showed excellent cycling performance. Compared to $Li[Ni_{0.8}Co_{0.2}]O_2$, $Li[Ni_{0.8}Co_{0.1}Mn_{0.1}]O_2$ exhibited greater thermal stability resulting from improved structural stability due to Mn substitution.

Keywords: Cathode material; Co-precipitation; Thermal stability; Lithium secondary batteries

1. Introduction

Sony researchers, who successfully commercialized lithium ion batteries, were the first to develop $LiCoO_2$ as a positive electrode material. Since then, a tremendous number of studies have been carried out all over the world to find the best material, optimize electrochemical properties, and understand the fundamental process involved in intercalation reactions. $LiNiO_2$ is a promising positive electrode due to its advantages over $LiCoO_2$. $LiNiO_2$ is less expensive, less toxic, and has a higher capacity than $LiCoO_2$. However, it has several problems, such as a difficult synthesis, low thermal stability, and poor cycle life in the charged state [1–9]. To overcome these problems, several cations have been substituted for Ni. Co doping on $LiNiO_2$ not only improves the layered characteristics of $LiNiO_2$, but it also increases thermal stability in the charged state. It has been reported that Co reduces cation mixing and improves structural stability. However, $Li[Ni_{1-y}Co_y]O_2$ has been found to exhibit low thermal stability and increased impedance during cycling, particularly at high temperatures [10–13].

In this study, the synthesis and electrochemical properties of spherical $Li[Ni_{0.8}Co_{0.2-x}Mn_x]O_2$ ($x = 0$, 0.1) are reported. The effects of substitution of Mn^{3+} for Co^{3+} in $Li[Ni_{0.8}Co_{0.2}]O_2$ on structure, electrochemical properties, and thermal stability are discussed.

2. Experimental

$[Ni_{0.8}Co_{0.1}Mn_{0.1}](OH)_2$ and $[Ni_{0.8}Co_{0.2}](OH)_2$ powders were prepared by co-precipitation [14]. An aqueous solution of $CoSO_4{\cdot}7H_2O$, $NiSO_4{\cdot}6H_2O$, and $MnSO_4{\cdot}5H_2O$ was pumped into a continuously stirred tank reactor (CSTR, capacity 4 L) under N_2 atmosphere. Simultaneously, a NaOH solution (aq) and an appropriate amount of NH_4OH solution (aq) as a chelating agent, were fed separately into the reactor. During the initial stage of the co-precipitation reaction, aggregated particles formed. With vigorous stirring, these particles grew into spherical particles.

The spherical $[Ni_{0.8}Co_{0.1}Mn_{0.1}](OH)_2$ and $[Ni_{0.8}Co_{0.2}](OH)_2$ powders were dried at 120 °C for 12 h to remove adsorbed water. Finally $[Ni_{0.8}Co_{0.2-x}Mn_x](OH)_2$ ($x = 0$, 0.1) was mixed with a stoichiometric amount of $LiOH{\cdot}H_2O$ and preheated to 480 °C for 5 h. It was then heated at 750 °C for 20 h to

* Corresponding author. Tel.: +82 2 2220 0524; fax: +82 2 2282 7329.
E-mail address: yksun@hanyang.ac.kr (Y.-K. Sun).

0378-7753/$ – see front matter © 2005 Elsevier B.V. All rights reserved.
doi:10.1016/j.jpowsour.2005.11.083

obtain spherical $Li[Ni_{0.8}Co_{0.1}Mn_{0.1}]O_2$ and $Li[Ni_{0.8}Co_{0.2}]O_2$ powders.

Powder X-ray diffraction (XRD) (Rigaku, Rint-2000) using Cu Kα radiation was used to identify the crystalline phase of the prepared powders at each stage. The morphology of the prepared powders was also observed using scanning electron microscopy (SEM, JSM-6340F, JEOL). The chemical composition of Ni, Co, and Mn for $[Ni_{0.8}Co_{0.2-x}Mn_x](OH)_2$ ($x = 0$, 0.1) was analyzed by atomic absorption spectroscopy (AAS, Vario 6, Analyticjena).

Charge–discharge tests were performed with a coin-type cell (CR2032) by applying a current density of 20 mA g^{-1} at 30 °C. A porous polypropylene film separated the positive electrode and the lithium metal negative electrode. For the fabrication of the positive electrode, a mixture containing 20 mg of active material and 5 mg of conducting binder (3.3 mg of teflonized acetylene black (TAB) and 1.7 mg of graphite) was pressed onto a 2.0 cm^2 stainless screen at 500 kg cm^{-2}. The electrolyte was a 1:1 mixture of ethylene carbonate (EC) and diethyl carbonate (DEC) containing 1 M $LiPF_6$ by volume (Cheil Industries Inc., Korea).

The long cycle-life tests were performed in a laminated-type full cell wrapped with an Al pouch (thickness: 1.5 mm, width: 40 mm, length: 60 mm and capacity: 110 mAh). Mesocarbon microbeads (MCMB 2528) were used as the negative electrode material. The fabrication of the cell was done in a dry room. Differential scanning calorimetry (DSC) experiments were carried out for the positive electrode materials by fully charging the coin cell to 4.3 V at a constant current and constant voltage, and opening it in an Ar-filled dry room. Measurements were carried out in a Pyris 1 differential scanning calorimeter (NETZSCH-TA4, Germany) with a temperature scan rate of 5 °C min^{-1}.

3. Results and discussion

The SEM images in Fig. 1 show that synthesized $[Ni_{0.8}Co_{0.1}Mn_{0.1}](OH)_2$ and $[Ni_{0.8}Co_{0.2}](OH)_2$ powders have spherical morphology without observable pores. The average particle size was estimated at 10–15 μm in diameter and the size-distribution was almost mono-dispersed, as shown in Fig. 1(a and c).

The measured cation ratios of Ni:Co:Mn in $[Ni_{0.8}Co_{0.1}Mn_{0.1}](OH)_2$ and $[Ni_{0.8}Co_{0.2}](OH)_2$ were 0.797:0.102:0.101 and 0.796:0.204:0, respectively. From the morphology and composition data, it could be inferred that $Ni(OH)_2$, $Co(OH)_2$, and $Mn(OH)_2$ co-precipitated homogeneously.

Fig. 2 shows the X-ray diffraction patterns for the $[Ni_{0.8}Co_{0.1}Mn_{0.1}](OH)_2$ and $[Ni_{0.8}Co_{0.2}](OH)_2$ powders. The spectra of $[Ni_{0.8}Co_{0.1}Mn_{0.1}](OH)_2$ and $[Ni_{0.8}Co_{0.2}](OH)_2$ compounds is similar to the spectra of pure β-$Ni(OH)_2$ [15]. All diffraction lines are indexed to a hexagonal structure with a space group of $p\bar{3}m1$. Table 1 lists the lattice parameters (a and c) of $[Ni_{0.8}Co_{0.1}Mn_{0.1}](OH)_2$ and $[Ni_{0.8}Co_{0.2}](OH)_2$ that were calculated from Fig. 2. This result showed that Co^{2+} and Mn^{2+} partially substituted for Ni^{2+} in the $Ni(OH)_2$ structure.

The SEM images of $Li[Ni_{0.8}Co_{0.1}Mn_{0.1}]O_2$ and $Li[Ni_{0.8}Co_{0.2}]O_2$ in Fig. 3 show that the spherical morphology of particles was maintained even after the thermal

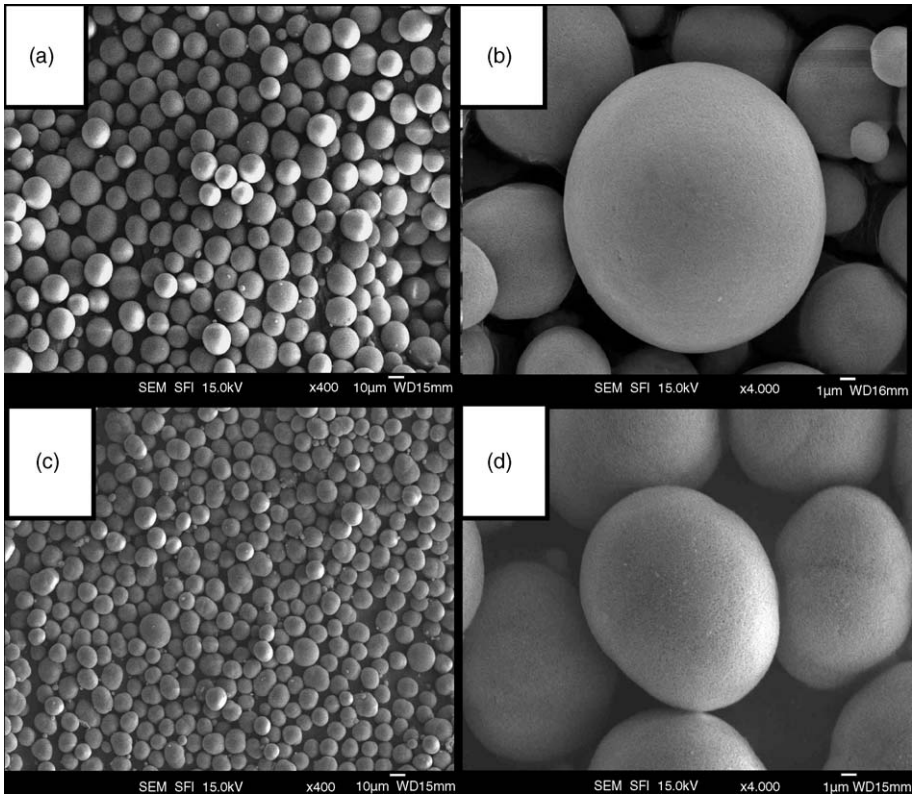

Fig. 1. SEM images: (a) low- and (b) high-magnification of pristine $[Ni_{0.8}Co_{0.1}Mn_{0.1}](OH)_2$; (c) low- and (d) high-magnification of $[Ni_{0.8}Co_{0.2}](OH)_2$.

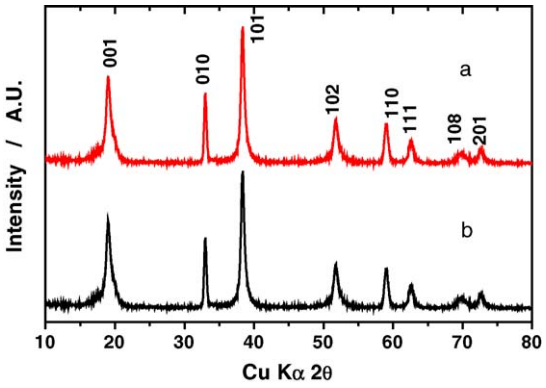

Fig. 2. XRD pattern of (a) $[Ni_{0.8}Co_{0.1}Mn_{0.1}](OH)_2$ and (b) $[Ni_{0.8}Co_{0.2}](OH)_2$ powders.

Table 1
Comparison of lattice parameters of $[Ni_{0.8}Co_{0.1}Mn_{0.1}](OH)_2$ and $[Ni_{0.8}Co_{0.2}](OH)_2$ powders

	a (Å)	c (Å)
$[Ni_{0.8}Co_{0.1}Mn_{0.1}](OH)_2$	3.1322	4.6544
$[Ni_{0.8}Co_{0.2}](OH)_2$	3.1298	4.6434

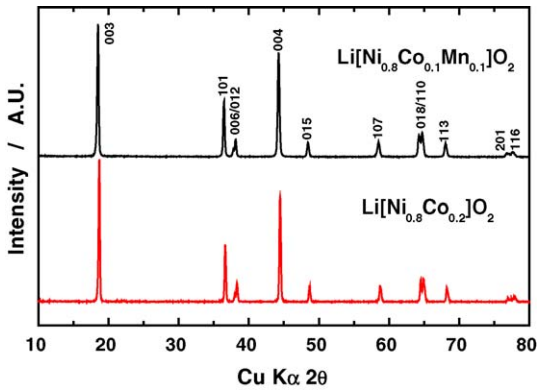

Fig. 4. XRD pattern of $Li[Ni_{0.8}Co_{0.1}Mn_{0.1}]O_2$ and $Li[Ni_{0.8}Co_{0.2}]O_2$ powders.

Table 2
Comparison of lattice parameters of $Li[Ni_{0.8}Co_{0.1}Mn_{0.1}]O_2$ and $Li[Ni_{0.8}Co_{0.2}]O_2$ powders

	a(Å)	c(Å)	c/a	Volume
$Li[Ni_{0.8}Co_{0.1}Mn_{0.1}]O_2$	2.8687	14.2531	4.9685	101.58
$Li[Ni_{0.8}Co_{0.2}]O_2$	2.8658	14.2482	4.9718	101.34

treatment process. The final compositions of Li:Ni:Co:Mn for the two powders were 0.99:0.795:0.103:0.102 and 0.98:0.767:0.233:0, respectively. After thermal treatment, a space group of $[Ni_{0.8}Co_{0.1}Mn_{0.1}](OH)_2$ and $[Ni_{0.8}Co_{0.2}](OH)_2$ changed to $R\dot{3}m$ structure, as seen in Fig. 4. The XRD patterns of $Li[Ni_{0.8}Co_{0.1}Mn_{0.1}]O_2$ and $Li[Ni_{0.8}Co_{0.2}]O_2$ powders showed a high degree of crystallinity and a hexagonal doublet (1 0 8)–(1 1 0) with a clear splitting. The lattice parameters (a, c, c/a) and unit cell volume of $Li[Ni_{0.8}Co_{0.2-x}Mn_x]O_2$ ($x = 0$, 0.1) are summarized in Table 2. When Mn is substituted for Co, the lattice parameters of a and c increased from 2.8658

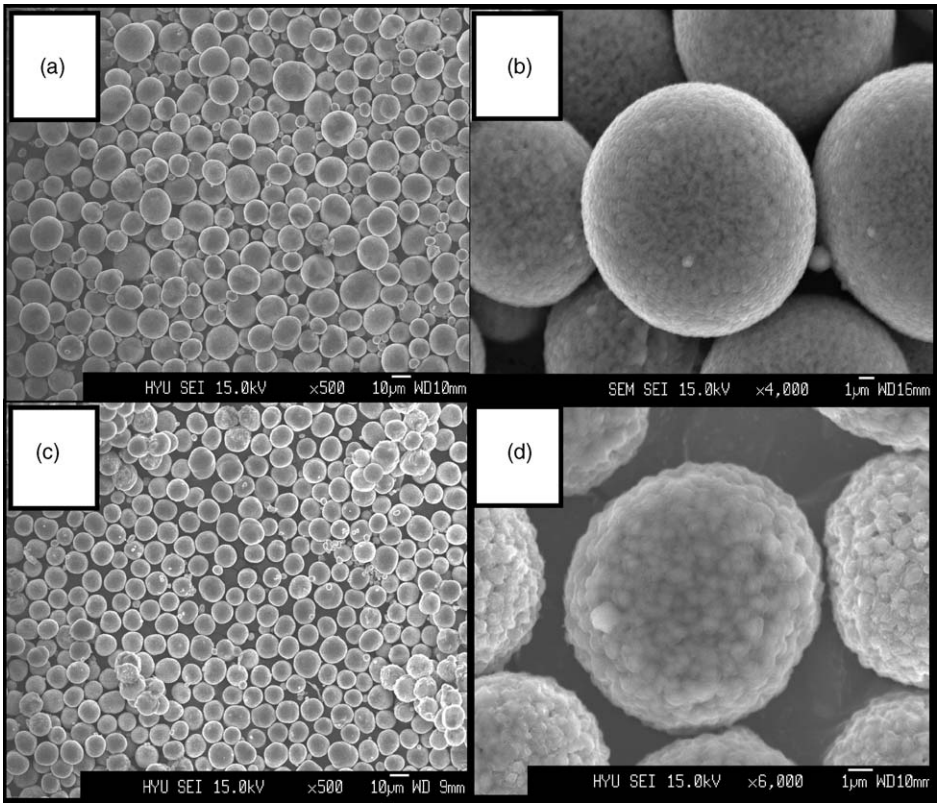

Fig. 3. SEM images: (a) low- and (b) high-magnification of pristine $Li[Ni_{0.8}Co_{0.1}Mn_{0.1}]O$; (c) low- and (d) high-magnification of $Li[Ni_{0.8}Co_{0.2}]O_2$.

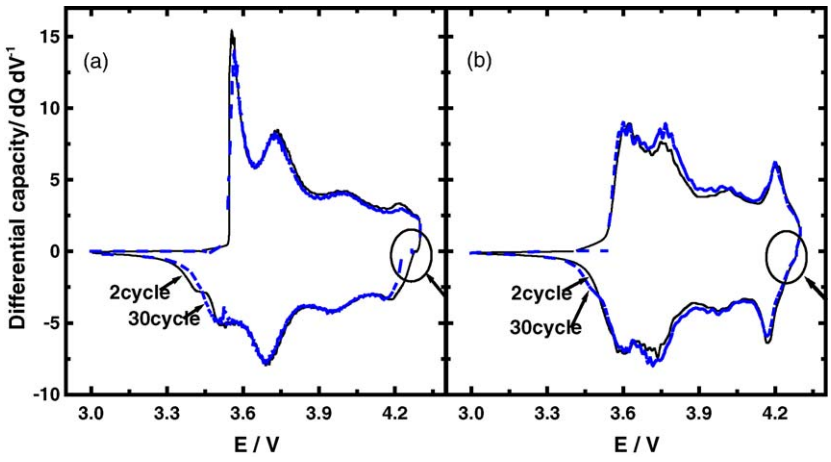

Fig. 5. Differential capacity vs. voltage of (a) Li/Li[$Ni_{0.8}Co_{0.2}$]O_2 and (b) Li/Li[$Ni_{0.8}Co_{0.1}Mn_{0.1}$]O_2 cell at the voltage range of 3.0–4.3 V.

to 2.8687 Å and from 14.2482 to 14.2531 Å, respectively. This can be attributed to the larger size of Mn^{3+} (0.645Å) compared to Co^{3+} (0.545Å). Due to the increase of lattice parameters, the *c*/*a* ratio of Li[$Ni_{0.8}Co_{0.1}Mn_{0.1}$]O_2 is smaller than that of Li[$Ni_{0.8}Co_{0.2}$]O_2, and unit cell volume increased from 101.34 to 101.58 $Å^3$ with substitution of Mn.

Fig. 5 shows the differential capacity (d*Q*/d*V*) versus voltage profiles of the 2nd and 30th cycle for Li/Li[$Ni_{0.8}Co_{0.2-x}Mn_x$]O_2 ($x = 0$, 0.1) cells. The cells were cycled between 3.0 and 4.3 V at a constant current density of 20 mA g^{-1} (0.4 mA cm^{-2}). For Li[$Ni_{0.8}Co_{0.2}$]O_2, a sharp peak appeared at 3.56 V and several other peaks appeared (3.73, 4.02 and 4.23 V) during charging that are a result of multiphase transitions. The sharp and broad peaks indicate first-order phase transition*s* (two-phase co-existence) and one-phase transitions, respectively [1]. On charging, Mn substitution causes the first peak shift to higher voltage (from 3.56 to 3.6 V) and a decrease in the peak intensity and sharpness. This implies that Mn substitution suppressed the undesired first-order phase transition during cycling [16–18]. Compared to Li[$Ni_{0.8}Co_{0.2}$]O_2, the two distinct redox peaks of Li[$Ni_{0.8}Co_{0.1}Mn_{0.1}$]O_2 at 4.2 V on charging and 4.16 V on discharging are possibly associated with the participation of Mn ion [19]. There is no significant difference in peak degradation between the 2nd and 30th cycles for Li[$Ni_{0.8}Co_{0.2}$]O_2 and Li[$Ni_{0.8}Co_{0.1}Mn_{0.1}$]O_2. However, for Li[$Ni_{0.8}Co_{0.2}$]O_2, a slight decrease of the redox peak area near 4.25 V (indicated with arrow) was observed, suggesting that capacity loss of the material could be occurring during cycling. Therefore, it could be concluded that Mn substitution improved structural stability and electrochemical properties. This result well consistent with the thermal stability of the Li[$Ni_{0.8}Co_{0.1}Mn_{0.1}$]O_2 shown in Fig. 9.

Fig. 6 shows capacity–voltage plots for the first cycle in the voltage range of 3.0–4.3 V at a constant current density of 20 mA g^{-1}. The Li[$Ni_{0.8}Co_{0.1}Mn_{0.1}$]O_2 and Li[$Ni_{0.8}Co_{0.2}$]O_2 delivered an initial discharge capacity of 198 and 203 mAh g^{-1} at 0.1 C-rate, respectively. The subtle decrease of discharge capacity is attributed to the increase of discharge voltage by Mn substitution. Less lithium will be intercalated at the same cut-off voltage when Mn has been substituted [20].

The mechanism of irreversible capacity at the 1st cycles is generally considered to be due to the irreversible oxidation of the extra Ni^{2+} during the first charge, thus inducing a local shrinking of the structure and hindering lithium re-intercalation [21]. There is no significant difference in the irreversible capacity loss of 12–14% between Li[$Ni_{0.8}Co_{0.1}Mn_{0.1}$]O_2 and Li[$Ni_{0.8}Co_{0.2}$]O_2. The discharge voltage of Li/Li[$Ni_{0.8}Co_{0.1}Mn_{0.1}$]O_2 is higher than that of Li/Li[$Ni_{0.8}Co_{0.2}$]O_2, which is consistent with the increase in peak intensity near 4.2 V, shown in Fig. 5.

Fig. 7 shows the plot of discharge capacity versus cycling number in the voltage range of 3.0–4.3 V at the 0.1 C-rate (20 mA g^{-1}) for 1–10 cycles and finally at the 0.2 C-rate (40 mA g^{-1}) for 10–60 cycles. The test result showed that Li[$Ni_{0.8}Co_{0.1}Mn_{0.1}$]O_2 exhibits better capacity retention, 94%, than that of Li[$Ni_{0.8}Co_{0.2}$]O_2 after 50 cycles. This result is consistent with the conclusion of Yoshio [22], who stated that as Mn ions are substituted in the Li[$Ni_{1-x}Mn_x$]O_2 structure, the structure stabilizes.

To observe long-term cycling properties, a carbon electrode was used as the negative electrode. Laminated-type lithium ion batteries using an Al pouch with a capacity of

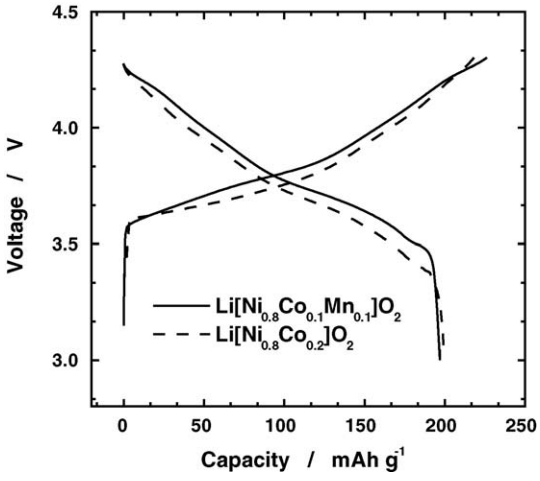

Fig. 6. The initial charge–discharge curves of Li/Li[$Ni_{0.8}Co_{0.1}Mn_{0.1}$]O_2 and Li/Li[$Ni_{0.8}Co_{0.2}$]O_2 cell in the voltage range of 3.0–4.3 V.

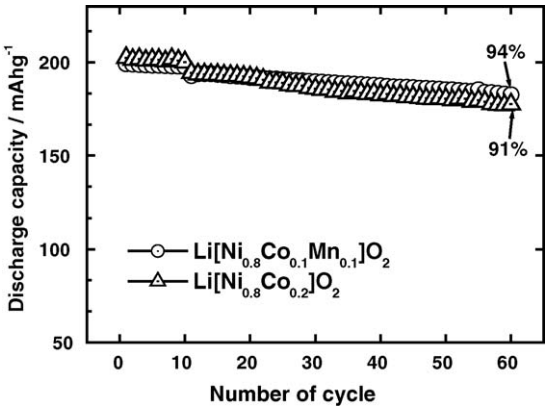

Fig. 7. Specific discharge capacity vs. cycling number for Li/Li-$[Ni_{0.8}Co_{0.1}Mn_{0.1}]O_2$ and Li/Li$[Ni_{0.8}Co_{0.2}]O_2$ cell in the voltage range of 3.0–4.3 V.

approximately 110 mAh were assembled. The fabricated cells were charged and discharged for 300 cycles at 1 C-rate between 3.0 and 4.3 V shown in Fig. 8. Although $Li[Ni_{0.8}Co_{0.1}Mn_{0.1}]O_2$ needed the first few cycles for activation, the cycling performance of C/$Li[Ni_{0.8}Co_{0.1}Mn_{0.1}]O_2$ cell is better than that of C/$Li[Ni_{0.8}Co_{0.2}]O_2$ at high rate. The C/$Li[Ni_{0.8}Co_{0.1}Mn_{0.1}]O_2$ cell showed a capacity retention of 85% compared to its maximum discharge capacity. The enhanced cycling stability can be attributed to the suppression of first-order phase transitions during charge–discharge as described in Fig. 5.

The thermal stability of positive materials, especially in the delithiated state, is an important factor in judging their suitability for practical applications in lithium secondary batteries. Fig. 9 shows the differential scanning calorimetry profiles of $Li[Ni_{0.8}Co_{0.1}Mn_{0.1}]O_2$ and $Li[Ni_{0.8}Co_{0.2}]O_2$ in the charged state to 4.3 V. The DSC experiments were made in welded and scaled stainless steel tubes so that no leaking of pressurized electrolyte was possible. The main peak temperature and exothermic peak area of $Li[Ni_{0.8}Co_{0.2}]O_2$ was 209 °C and 5675 J g^{-1}, respectively. The thermal stability of $Li[Ni_{0.8}Co_{0.1}Mn_{0.1}]O_2$ was significantly enhanced. Its DSC profile exhibited a relatively small peak at 219 °C and the generated heat was only 2763 J g^{-1}. The oxidation state of the transition metal ions (Ni, Co, Mn) in $Li[Ni_{0.8}Co_{0.1}Mn_{0.1}]O_2$ is believed to be 3+ [23,24]. If all of the Li^+ ions in $Li[Ni_{0.8}Co_{0.1}Mn_{0.1}]O_2$ were deintercalated from the lattice, the oxidation state of the Ni, Co, and Mn would be changed to 4+. It is well known that delithiated $Li_{1-x}NiO_2$ cathode material with a high oxidation state Ni^{4+} will evolve oxygen at elevated temperatures and induce exothermic decomposition reactions between cathode and electrolyte [25]. It has been also reported that the stable oxidation number of Mn ion is 4+. Hence, due to Mn^{4+}, the thermal characteristics of $Li_{1-x}[Ni_{0.8}Co_{0.1}Mn_{0.1}]O_2$ after charging could be more stable than that of $Li[Ni_{0.8}Co_{0.2}]O_2$.

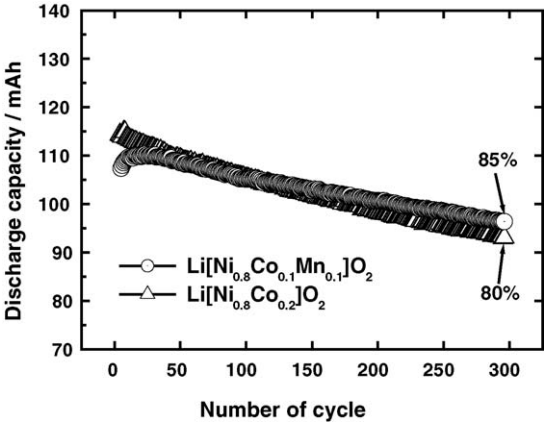

Fig. 8. Discharge capacity vs. cycling number of C/$Li[Ni_{0.8}Co_{0.1}Mn_{0.1}]O_2$ and C/$Li[Ni_{0.8}Co_{0.2}]O_2$ cell at the voltage range of 3.0–4.3 V.

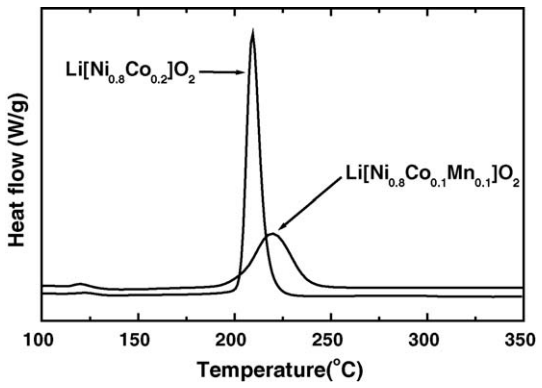

Fig. 9. Differential scanning calorimetry traces of $Li[Ni_{0.8}Co_{0.1}Mn_{0.1}]O_2$ and $Li[Ni_{0.8}Co_{0.2}]O_2$ cell at charged state to 4.3 V.

4. Conclusion

Spherical, mono-disperse, and phase-pure $Li[Ni_{0.8}Co_{0.2-x}Mn_x]O_2$ ($x = 0$, 0.1) powders with high crystallinity and an average particle size of approximately 10–15 μm in diameter were synthesized from $LiOH{\cdot}H_2O$ and co-precipitated the spherical metal hydroxide, $[Ni_{0.8}Co_{0.2-x}Mn_x](OH)_2$ ($x = 0, 0.1$). Although the $Li[Ni_{0.8}Co_{0.1}Mn_{0.1}]O_2$ delivered a somewhat lower initial discharge capacity, the capacity retention and thermal stability were improved compared with $Li[Ni_{0.8}Co_{0.2}]O_2$. The enhanced electrochemical properties could be attributed to the stabilization of the host structure via Mn substitution for Co.

Acknowledgements

This work was supported by KOSEF through the Research Center for Energy Conversion and Storage and the Core Technology Development Program of the Ministry of Commerce, Industry and Energy (MOCIE).

References

[1] T. Ohzuku, A. Ueda, M. Nagayama, J. Electrochem. Soc. 140 (1993) 1862.
[2] K. Sckai, H. Azuma, A. Omaru, S. Fujita, J. Power Sources 43 (1993) 241.
[3] M. Broussely, F. Perton, J. Labat, R.J. Staiewiez, A. Romero, J. Power Sources 43 (1993) 209.
[4] J.R. Dahn, U. von Sacken, M.W. Juzkow, H. Ai-janab, J. Electrochem. Soc. 138 (1991) 2270.
[5] T. Miyashita, H. Noguchi, K. yamato, M. Yoshio, J. Ceram. Soc. Jpn. 102 (1994) 58.
[6] C. Delmas, I. Saadoune, Solid State Ionics 53–56 (1992) 370.

[7] A. Ueda, T. Ohzuku, J. Electrochem. Soc. 141 (1994) 2010.
[8] R. Alcantara, P. Lavela, J.L. Tirado, R. Stoyanova, E. Zhecheva, J. Electrochem. Soc. 145 (1998) 730.
[9] J. Cho, G. Kim, H.S. Lim, J. Electrochem. Soc. 146 (1999) 3571.
[10] J. Cho, H. Jung, Y. Park, G. Kim, H. Lim, J. Electrochem. Soc. 147 (2000) 15.
[11] Y. Gao, M.V. Yakovleva, W.B. Ebner, Electrochem. Solid State Lett. 1 (1998) 117.
[12] K. Kubo, S Arai, S. Yamada, M. Kanda, Abstracts of the Ninth International Meeting on Lithium Batteries, Edinburge, Scotland, July 12–17, 1998.
[13] S. Ishida, A. Sugimoto, K. Hanawa, in: Proceedings of the 38th Battery Symposium in Japan, The Electrochemical Society of Japan, November 11–13, 1997, p. 101.
[14] M.-H. Lee, Y.-J. Kang, S.-T. Myung, Y.-K. Sun, Electrochem. Acta 50 (2004) 939.
[15] J. Ying, C. Wan, C. Jiang, Y. Li, J. Power Sources 99 (2001) 78.
[16] C. Delmas, M. Menetrier, L. Croguennec, I. Saadoune, A. Rouger, C. Pouillerie, G. Prado, M. Grune, L. Fournes, Electrochim. Acta 45 (1999) 243.
[17] X.Q. Yang, X. Sun, J. MvBreen, Eletrochem. Commun. 2 (2000) 733.
[18] K.K. Lee, K.B. Kim, J. Electrochem. Soc. 147 (2000) 1709.
[19] Y. Chen, G.X. Wang, K. Konstantinov, H.K. Liu, S.X. Dou, J. Power Sources 119–121 (2003) 184.
[20] H. Liu, J. Li, Z. Zhang, Z. Gong, Y. Yang, Electrochim. Acta 49 (2004) 1151.
[21] A. Rougier, P. Gravereau, C. Delmas, J. Electrochem. Soc. 143 (1996) 1168.
[22] M. Yoshio, Y. Todorov, K. Yamato, H. Noguchi, J.-I. Itoh, M. Okada, T. Mouri, J. Power Sources 74 (1998) 46.
[23] M. Yoshio, H. Noguchi, J. Itoh, M. Okada, T. Moure, J. Power Sources 90 (2000) 176.
[24] D. Carlier, M. Menetrier, C. Delmas, J. Mater. Chem. 11 (2001) 594.
[25] H. Arai, S. Okada, Y. Sakurai, J. Yamaki, Solid State Ionics 109 (1998) 29.